Nuclear Medicine and Molecular Imaging (2020) 54:65–80
https://doi.org/10.1007/s13139-020-00635-w

REVIEW

ISSN (print) 1869-3482
ISSN (online) 1869-3474

New Frontiers in Molecular Imaging with Superparamagnetic Iron Oxide Nanoparticles (SPIONs): Efficacy, Toxicity, and Future Applications

Viviana Frantellizzi[1] · Miriam Conte[2] · Mariano Pontico[3] · Arianna Pani[4] · Roberto Pani[5] · Giuseppe De Vincentis[2]

Received: 4 November 2019 / Revised: 23 December 2019 / Accepted: 22 January 2020 / Published online: 8 February 2020

Abstract

Supermagnetic Iron Oxide Nanoparticles (SPIONs) are nanoparticles that have an iron oxide core and a functionalized shell. SPIONs have recently raised much interest in the scientific community, given their exciting potential diagnostic and theragnostic applications. The possibility to modify their surface and the characteristics of their core make SPIONs a specific contrast agent for magnetic resonance imaging but also an intriguing family of tracer for nuclear medicine. An example is 68Ga-radiolabeled bombesin-conjugated to superparamagnetic nanoparticles coated with trimethyl chitosan that is selective for the gastrin-releasing peptide receptors. These receptors are expressed by several human cancer cells such as breast and prostate neoplasia. Since the coating does not interfere with the properties of the molecules bounded to the shell, it has been proposed to link SPIONs with antibodies. SPIONs can be used also to monitor the biodistribution of mesenchymal stromal cells and take place in various applications. The aim of this review of literature is to analyze the diagnostic aspect of SPIONs in magnetic resonance imaging and in nuclear medicine, with a particular focus on sentinel lymph node applications. Moreover, it is taken into account the possible toxicity and the effects on human physiology to determine the SPIONs' safety.

Keywords SPION · Iron oxide nanoparticles · Review · 68Ga-radiolabeled bombesin · Molecular imaging

Introduction

Superparamagnetic iron oxide nanoparticles (SPIONs) are crystals of iron oxide called magnetite (Fe_3O_4) or maghemite (Fe_2O_3) with a shell that can be modified to gain stability in aqueous media and to modify the biochemical properties for various use in biomedical fields [1, 2]. They have a diameter ranged from 20 to 150 nm and sensitivity to a magnetic field that makes them useful as contrast agent in magnetic resonance imaging (MRI) and for various medical applications. For the capacity not to influence the properties of antibodies, SPIONs could be used conjugated with antibodies to track tumoral cells. Examples are anti-mesothelin antibodies for pancreatic adenocarcinoma [3], anti-insulin-like-growth-factor binding protein 7 (anti-IGFBP-7) antibodies in glioblastoma [4], and anti-CD44 antibodies used in breast cancer (BC) [5]. On the other side, the applications of SPIONs as contrast agents are different: in magnetic particle imaging, as agent coated with folate to induce a negative contrast in HeLa cells that are positive for the folate receptors and as tracers in magnetic particle imaging [6]. A particular type of SPIONs has been developed, Nanomag, to reveal the mesenchymal stromal cells biodistribution in osteochondral injuries [7]. In urologic oncology, SPIONs are injected in peritumoral or into the primary tumor for the identification of the sentinel lymph node (SLN) such as penile cancer and prostate cancer in all its variant [8, 9]. Also, in BC could help identify SLN [10–13]. Despite all, SPIONs have an impact on the cellular

✉ Viviana Frantellizzi
viviana.frantellizzi@uniroma1.it

1 Department of Molecular Medicine, Sapienza University of Rome, Viale Regina Elena 324, 00161 Rome, Italy

2 Department of Radiological Sciences, Oncology and Anatomical Pathology, Sapienza University of Rome, Rome, Italy

3 Program in Morphogenesis & Tissue Engineering, Sapienza University of Rome, Rome, Italy

4 Department of Oncology and Hemato-oncology, Statale University of Milan, Milan, Italy

5 Department of Medico-Surgical Sciences and Biotechnologies, University La Sapienza, Rome, Italy

viability in BC, hinder the neovascularization and induce autophagy in endothelial progenitor cells [14, 15]. They could be responsible for injuries on Deoxyribonucleic Acid (DNA), mitochondrion, actin, on regulatory proteins of the cellular cycle, and on proteins engaged in the transduction of the intracellular signal. They could interfere also with the iron homeostasis [16, 17]. Furthermore, some authors demonstrated that in aqueous media they could be unstable and the particles tend to aggregate [14]. There are, also, very few studies in vitro on SPIONs that are not exhaustive to determinate the complete safety of SPIONs utilization on humans. Numerous studies published in these last years have represented the advantages and disadvantages of the SPIONs. This review aims to summarize the principal uses in diagnostic imaging and explore the toxicity of SPIONs in comparison to the current gold standard radioisotope used in lymphoscintigraphy.

SPIONs: Definition and Physicochemical Properties

SPIONs are crystals constituted by a core of iron oxide and a surface that can be modified in various ways for different biomedical applications. For the diameter of the whole hydrated compound (core and shell), SPIONs can be classified in oral SPIONs, (diameter between 300 nm and 3.5 μm), standard SPIONs (which size is 50–150 nm), and ultra-small SPIONs (diameter smaller than 50 nm) [18, 19] (See Fig. 1). The ideal SPIONs for intravenous administration have a range of 10 to 100 nm. SPIONs with size < 10 nm or > 200 nm, instead, have a reticuloendothelial system (RES) clearance [16, 18]. This represents a restriction for their application, but some studies have revealed that the surface properties can influence their internalization in phagocytic cells. For example carboxydextran-coated SPIONs with range less of dextran-SPIONs ones are phagocyted by macrophages mostly than dextran-SPIONs. It was not associated to cell activation and interleukine-1 release. The particles with a radius greater than 100 nm are phagocytosed. When the particle size is under 30 nm, SPIONs are quickly taken up by pinocytosis [6]. Not only the size but also the modifications of the shell influence significantly the cellular uptake and intracellular pathways of SPIONs, crucial for medical applications. It is thought to cover SPIONs shell with organic acids (e.g., citric acid [20]), to cap it with semi-metallic compounds as silicate mesolayers [21]) or with hydrophilic polymers (e.g., poly(ethylene glycol) [1] and functionalized-polylactide (PLA) nanofibers [22]). Others polymers used are [2] dextran [23], chitosan [24], hyaluronic acid [25], and synthetic polymers like poly(ethylene glycol) (PEG) [26–28], polyamidoamine [29], polyglycerol [26], polyoxazoline [30], and poly(dimethylaminoethyl methacrylate) [31]. Also, polypeptides/polypeptoids have been considered as an alternative for SPIONs' shell coating [32, 33]. The shell modifications are obtained to guarantee the stability of SPIONs in water or in the physiological environment. The reason is blocking SPIONs aggregation and precipitation out of solutions. In fact, they have hydrophobic nature and they are opsonized in the bloodstream by blood proteins in order to facilitate aggregation [6, 22]. These strategies are also applied to get high local concentrations in determined tissues and to enhance the relaxivities of SPIONs [22].

Imaging Properties of SPIONs

Since MRI measures the change of magnetization of water protons after applying radiofrequency (RF) pulses, a contrast

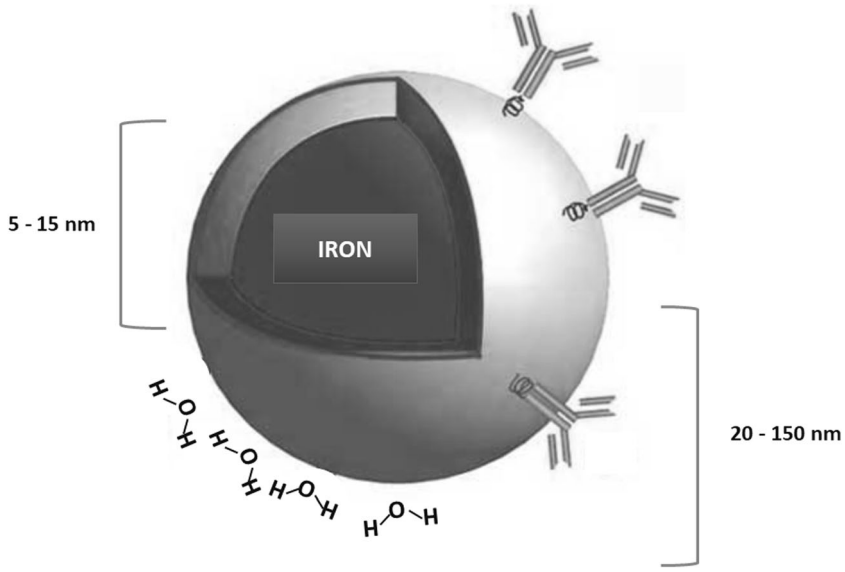

Fig. 1 The figure shows a supermagnetic iron oxide nanoparticle with a core (radius between 5 to15 nm) and the radius of the whole core with shell and water coat (from 20 to 150 nm)

agent can enhance the relaxation rate of water and it is defined relaxation rates. In fact, after the excitation of protons undergone to the RF pulses, the protons return to an equilibrium state, that is longitudinal T1 relaxation. The transfer of the spin angular momentum among protons is transfer (T2) relaxation. SPIONs behave as contrast agent, interact with surrounding water molecules and enhance the relaxation rate of water protons. The contrast agents shorten the T1 relaxation and/or T2 relaxation times. Commonly, SPIONs decrease the MR signal intensity of the regions where they are taken up, so those regions are seen darker in MRI [34, 35]. It is of interest to study the concentration of Fe_2^+ or Fe_3^+ ions in these compounds and how it changes the absorption at the surface of magnetite. We assert here that the zeta potential is a measure of the electric potential of the mineral surface. The electrostatic interactions of the mineral surface in solution, in particular, determine the entity and the sign of the zeta potential [36]. It is at the base of phenomena as flocculation and dispersion of a compound [37]. The high positive or negative zeta potential value is correlated to the dispersion stability of SPIONs as a consequence of electrostatic interactions [38]. Sun et al. [39] have shown that the zeta potential of magnetite decreased in acidic solutions and increased in basic solutions. When there is iron cations excess, specific adsorption has been seen at the surface of magnetite. It is related to its zeta potential. The iron oxides that represent the core of SPIONs are magnetite (-Fe_3O_4), maghemite (-Fe_2O_3), and hematite (-Fe_2O_3). They are characterized by a close-packed plane in which oxygen anion and iron cations are bound in an octahedral or tetrahedral crystalline system [40]. Maghemite contains Fe_2^+ and Fe_3^+ ions in a ratio of 1:2 and has ferrimagnetic properties in its natural state [6]. It has a cubic or tetrahedral geometry and defect spinel structural type. Two-thirds of its sites filled with Fe_3^+. Every two sites there is one vacant site. Magnetite has a ferromagnetic magnetism, a cubic crystallographic system and an inverse spinel structure. Fe_3^+ ions are distributed randomly between octahedral and tetrahedral sites, Fe_2^+ ions in octahedral sites. Hematite can have a low ferromagnetic or antiferromagnetic type of magnetism. It has a rhombohedral or hexagonal crystallographic system and a corundum structural type [40].

Magnetic Susceptibility of SPIONs

Iron oxide particles respond differently to an externally applied magnetic field, in fact, each particle has specific orientations of the magnetic moments [41]. To give some definitions, the magnetic behavior of iron oxides relies on four unpaired electrons in its 3d orbitals. The crystals of iron oxide have a different magnetic moment (M) and for that, they can exhibit ferromagnetic state, paramagnetic state, and antiferromagnetic state. In the ferromagnetic state, the single moment of each iron atom is aligned in an antiparallel way, independently from the presence of an external magnetic field. In ferromagnetic crystals, the iron atoms moments are antiparallel with different straight. If each iron moment has the same magnitude, the net crystal moment of ferrimagnetic crystals is equal to zero. It is because, conventionally, its vector M is calculated as the sum of the single moments of the iron atoms that form the crystal. Also, in the paramagnetic state, the net M is zero. However, it is related to the fact that single atom moments have the same magnitude and are aligned randomly with respect to each other. The particularity of ferromagnetic material is staying magnetized after removing the external magnetic field to which has been subjected before, describing the magnetic hysteresis loop, which is conventionally how to change the magnetic field in the function of the applied electric current. The residual magnetization after removing the external magnetic field can be explained because the atomic M stay aligned even in the absence of the magnetic field. Fe_3O^4 crystals with diameters equal or inferior to 20 nm, instead, are superparamagnetic because each crystal has its single magnetic domain in the external magnetic field and there is no hysteresis loop of their magnetization M. Maghemite and hematite in bulk are ferromagnetic and antiferromagnetic, respectively. In crystals conformations, they become superparamagnetic and act as magnetite. It explains the reason why SPIONs reveal their magnetic properties when they are in the magnetic field, at the opposite of what, for example, bulk magnetite shows. Furthermore, the magnetic properties of the magnetite are maintained even in the absence of an external magnetic field [6].

SPIONs as Contrast Agent or Tracer

SPIONs can be conjugated with tumor-specific antibodies (Ab) due to their binding capacity not to interfere with the proprieties of Ab itself and to gain specificity in targeting the tumor cells in the imaging techniques [6]. A summary of SPIONs' use, classified for molecular type, study's aim, type of population, and main results is shown in Table 1.

Mesothelin

As Ordóñez et al. described [58], mesothelin is a protein expressed on membranes by different malignancies such as adenocarcinoma of the pancreas, ampulla of Vater, endometrium, lungs and liver, cholangiocarcinoma, pancreatic ductal adenocarcinoma, the epithelial component of biphasic synovial sarcomas, ovarian non-mucinous carcinoma, and mesothelioma. It was therefore thought to bind SPIONs with Ab anti-mesothelin (A-MSF) to identify pancreatic carcinoma cells in mouse xenografts. The SPIONs were covered with silica shells [Fe_3O_4@ SiO_2 (FS)] to increase the biocompatibility of the tracer. Silica was chosen because of its non-

Table 1 Summary of the use of SPIONs classified for the molecular type, aim of the study and type of population considered for each study

Type of SPIONs	Aim of the study	Study population	Main results	References
A-MSF-SPIONs	To detect pancreatic carcinoma with MRI	Mouse	In T2-weighted images, the tumor signal decreased after administration. A-MSF-SPIONs may be a good T2 targeting agent in pancreatic cancer.	Shao C et al., 2016 [42]
Ab anti-IGDBP7-SPIONs	To identify abnormal glioblastoma vessel	Mouse	Selectivity in binding glioblastoma abnormal vessels seen in MRI, infrared imaging, histology, and fluorescence microscopy.	Tomanek B et al., 2012 [4]
folate-SPIONs micelles	To find cancer cells that overexpress CD44 HA-receptor (HeLa)	In vitro	HeLa cells showed a decreased signal intensity producing negative contrast in MRI. T2 relaxivity of the folate-SPIONs was equal to 260.4 mM-1 s-1 and it was observed higher internalization of folate-conjugated SPION–micelle formulations than the unconjugated micelles, features that make folate-SPIONs an auspicious T2-weighted MRI contrast agent.	Mahajan S et al., 2012 [43]
HA-SPIONs	SPIONs as T2-negative MRI contrast agent targeted for breast carcinoma cells that overexpress CD44 HA-receptor	In vitro	Decrease of T2 transverse relaxes time in HA-SPION-treated cells. HA-SPIONs could be used as a T2-negative MRI contrast agent in this cellular population.	Yang RM et al.,2017 [5]
Nanomag	To monitor the biodistribution of mesenchymal stromal cells (MSCs) in ovine osteochondral defect model	Sheep	The concentration of MSCs was evaluated histologically and with in vitro and ex vivo MRI: in vitro MRI highlighted a shortening of T2, while in ex vivo MRI the presence of nanoparticles was detected as a hypointense of the signal void region.	Markides H et al.,2019 [7]
Resovist	SPIONs as tracer in MPI to evaluate endovascular stenosis	Phantom	MRI could be able to recognize stenosis 2–9 mm with a spatial resolution of 1.5 mm × 3.0 mm × 3.0 mm.	Vogel P et al., 2014 [44] Vaalma S et al., 2017 [45]
Resovist	To localize SLN in breast cancer	Humans	SLN localized through transcutaneous and ex-vivo measurements with a handled-probe. Its longitudinal detection length was approximately 10 mm, for 140 μg of iron. In 5 patients on 6 SLNs were successfully detected.	Sekino M et al., 2018 [46]
Sienna+®	To localize SLN in early breast carcinoma	Humans	The sentinel detection rate was 95.6% for SPIONs and 96.9 for 99mTc. The nodal detection rate was 93.5 for SPIONs and 90.3 for 99mTc. In preoperative injection SPIONs had a better tracer-specific detection rate (95.3 versus 86% of 99mTc). The detection of SNB was better if blue dye was added to SPIONs injection.	Karakatsanis A et al., 2017 [13]
Sienna+®	To localize SLN in high risk PCa	Humans	Sienna+® tended to accumulate in lymph nodes let them detect at MRI as a T2-weighted strong drop of signal intensity regions. This technique had high sensitivity (96.6%), high specificity (95.6%), and high positive predictive value (96.6%); and negative predictive value (95.6%), low false negative rate (3.4%), and false positive rate (4.4%)	Winter A et al., 2017 [47]
Sienna+®	To localize SLN in high risk and intermediate risk of PCa	Humans	The results of preoperative MRI identification of SLN with intraoperative magnetometer-guided sLND had 100% diagnostic rate, sensitivity equal to 85.7%, 97.2% specificity, 92.3% positive predictive value, 94.9% negative predictive value, and 14.3% false negative rate.	Winter A et al., 2018 [10]
Sienna+®	To prove the equivalency of Sienna+® to 99mTc-Nanocoll® in breast cancer	Humans	The detection rate per patient for 99mTc was 97.3%, for Sienna+ 98%; nodal detection rate (proportion of sLN detected) was 91.8% for radioisotope, 97.3% for Sienna+. The malignancy detection rate per patient was 91.2% for radiopharmaceutical, 91.1% for SPIONs, and respectively per node 91.1% and 95.6%. The histological analysis conducted on LN removed gave positive results on 31/146 LN marked with isotope vs. 33/147 LN individuated with SPIONs.	Thill M et al., 2014 [48]
Sienna+®	To compare Sienna+® and 99mTc-Nanocoll® in breast cancer	Humans	Sentinel node identification was 95.0% with gold standard and 94.4% for SPIONs. The identification rate with gamma probe was 90.6%, with a discordance between the two methods of 6.9%. At histopathology, of 107 LN not detected by isotope, 55 were identified by Sienna+. 29 LN were identified by 99mTc-Nanocoll®only. SPIONs, however, was limited by false negative	Douek M et al., 2013 [49] Ahmed M et al., 2014 [50]

Table 1 (continued)

Type of SPIONs	Aim of the study	Study population	Main results	References
			because not all the lymph nodes identified were detected by gold standard.	
Sienna+®	To localize SNL in intermediate risk PCa	Humans	Sienna+® as an alternative to the gold standard to detect the SLN in intermediate and high risk PCa. They performed magnetometer-guided sLND gaining a diagnostic rate of 95%.	Stanik M et al., 2018 [11]
Ferumoxatran-10	To localize SLN in penile cancer	Humans	Hyperintense signal in metastatic LNS on T1 compared to normal tissue. At the opposite, non-metastatic sLN contained great quantitative of SPIONs. Tabatabei et al. reported 100% sensitivity, 97% specificity, 81.2% positive predictive value, and 100% negative predictive value for this technique.	Mehralivand S et al., 2018 [12] Tabatabaei S et al., 2005 [51]
99mTc-Fe3O4-HEDP-MNPS	Theragnostic nanoagent (bone uptake)	Mice	After injection in mice tail veins of 99mTc-Fe3O4-HEDP MNPs and 99mTc-HEDP, dynamic SPECT studies and planar imaging were acquired by gamma camera with Low energy-High resolution with energy peak setting on 140 keV: MNPs accumulated in liver and spleen and eliminated by the urinary system; 99mTc-HEDP, at the opposite side, showed bone uptake.	Mirković M et al., 2019 [52]
68Ga-DOTA-BN-TMC-MNPs	To detect breast cancer cells	Mice	The images T2-weighted images of tumor lesion appeared darker since the improved contrast. The tracer in aqueous solutions expressed decreased signal intensity at the Fe concentration surge, and the T2 relaxivity (r2) estimated was 330.98 mM−1 s^−1. 68Ga labeling of DOTA–BN–TMC–MNPs was evaluated with PET. It showed high sensitivity and better visibility of tumor at a lower concentration of NPs (0.62 mg/mL) than MRI.	Lee CM et al., 2010 [53] Hajiramezanali M et al., 2019 [54]
ALMs- SPIONs	To target stem cells for the treatment of lung disease	Rats	Hyperpolarized 129 Xe MRI was used to detect SPION-labeled ALMs in the airways after 1 hour. The areas, in which SPION-labeled ALMs localized, appaired as regions of signal loss with a T∗2 decreased to 54.0 ± 7.0% of the baseline after an hour.	Riberdy V et al. [55] 2019
EGFRvIII -NHS-PEG-SPIONs	To target, as nanoprobe, areas of EGFRvIII-positive glioblastoma	Mice	The brain tumor region appaired as a strong signal area. Fluorescence imaging revealed that areas of major fluorescence intensity in the brain of the mice injected the SPIONs compared to control mice.	Liu X et al., 2019 [56]
PLGA-PEG-SPIONs	To detect tumor cells expressing EGFR	In vitro	This compound showed a good water-solubility, stability, and biocompatibility. Useful synthesized nanoprobe for negative contrast enhancement.	Salehnia Z et al. 2019 [57]

toxicity and stability. The authors of the study observed that A-MFS could be used as a contrast agent since the T2 relaxation rate was 59.435 mM/s and its T1 relaxation rate 0.549 mM/s. In T2-weighted images, the tumor signal decreased after injection of the probe FS associated with A-MSF. For that, FS with A-MSF could be considered a good T2 targeting agent in pancreatic cancer of nude mice [42].

Anti-IGFBP7

In another application, SPIONs linked with anti-IGFBP7 were used to recognize the abnormal vessel that irrorates the glioblastoma [4]. The IGFBP7 is a protein expressed by tumor cells [59], in particular in the tumor blood vessel and in low or none quantitative in the normal vessel [60–62]. The expression of IGFBP7 is not dependent on the tumor size, otherwise, VEGFR seems to be related to the growing of the tumor [63]. Thus, the IGFBP7 turned out a good candidate to combine with SPIONs. In this study, SPIONs were coated with dextran, linked with Ab anti-IGFBP7 and used in a mouse model of glioblastoma. MRI, infrared imaging, histology, and fluorescence microscopy have demonstrated the selectivity of the nanoparticles in binding glioblastoma abnormal vessels.

HA-SPIONs

In mammalian carcinoma, hyaluronan (HA)-modified superparamagnetic iron oxide nanoparticles (HA-SPIONs) has been proposed as a diagnostic T2-negative MRI contrast

agent targeted for BC cells that overexpress CD44 HA-receptor. In uptake studies with Prussian blue staining method, the cells that internalized the Fe_3O_4 took on the typical blue color. With MRI, it was seen a decrease of T2 transverse relax times in HA-SPION-treated cells. This suggests that HA-SPIONs could be used as a T2-negative MRI contrast agent in these cellular populations [5]. Alike, HeLa cells, a cervical carcinoma cell line that is positive for folate receptors, were treated with folate-SPIONs micelles. They showed a decreased signal intensity producing negative contrast in MRI. Given that alpha-isoform of the folate receptor is overexpressed in several epithelial origin cancers and has a limited expression in normal tissues, it is a specific tumor marker for these malignancies. For that folate-SPIONs was studied as contrast agent in MRI: the high T2 relaxivity of the folate-SPIONs (260.4 mM-1 s-1) and the higher internalization of folate-conjugated SPION–micelle formulations than the unconjugated micelles was an auspicious T2-weighted MRI contrast agent for cancer imaging [43].

Nanomag

SPIONs were used to monitor the biodistribution of mesenchymal stromal cells (MSCs) in ovine osteochondral defect model. The ovine MSCs were labeled with Nanomag, a type of 250 nm SPIONs with a -COOH tail, using the cell-penetrating peptide P21-8R and glycosaminoglycan-binding enhanced transduction (GET). It was created a surgically osteochondral defect in the medial femoral condyle (MFC) of the left stifle joints and then GET-Nanomag-labeled autologous mesenchymal cells were injected in the joints of the sheep. The concentration of MSCs was evaluated histologically and with in vitro and ex vivo MRI: in vitro MRI highlighted a shortening of T2, while in ex vivo MRI the presence of nanoparticles was detected as a hypointense of the signal void region [7].

Resovist (Ferucarbotran)

Resovist (ferucarbotran), a type of SPIONs polydisperse and coated with negatively charged 60 nm carboxydestran shell that stabilizes the magnetic aggregation [46, 64], could be used as tracers in magnetic particle imaging thanks to their magnetic characteristics that allow obtaining anatomical details and three-dimensional images of its distribution in the tissues with a good contrast [44]. For its sensitivity and high signal-to-noise ratio and for its signal proportional to the concentration in the tissue, it has been proposed as tracer in cardiovascular imaging to evaluate the stenosis. Vaalma et al. reproduced a different type of stenosis with the aid of ten vascular phantoms each other different for their diameters. After filling the phantoms with Resovist, they have performed MRI that could be able to recognize stenosis 2–9 mm with a spatial resolution of 1.5 mm × 3.0 mm × 3.0 mm [45]. Resovist can also be used in mammalian carcinoma. After the injection of this tracer into the subareolar region and the following massage of the injection site to promote lymphatic drainage of SPIONs, the surgeon with a handled magnetic probe located the SLN. After the biopsy of the SLN, scanning with a magnetic probe was performed to confirm the absence of SLNs in the axilla (the signal should be less than 1 mcT) [46].

SPIONs for Sentinel Lymph Node

Remaining in the BC field, MONOS trial had demonstrated that SPIONs can be used in alternative to the gold standard ^{99}mTc (with or without blue dye) to individuate the SLN in early BC with better results compared to perioperative injection. They used Sienna+®, a carboxydestran coated and hydrodynamic of 60 nm. The sentinel detection rate was 95.6% for SPIONs and 96.9% for 99mTc and the nodal detection rate was 93.5% for SPIONs and 90.3% for ^{99}mTc, but in preoperative injection SPIONs had a better tracer-specific detection rate (95.3% versus 86% of ^{99}mTc). The detection of SLB was better if blue dye was added to SPIONs injection [13]. In a study conducted by Winter et al., Sienna+® was injected peritumorally through transrectal ultrasound guidance 24 h before surgery and used as a tracer with a handheld magnetometer (SentiMag®). This system combined with sentinel lymph node dissection (SLND) could be helpful to detect SLN in high-risk prostatic cancer (PCa) patients. In spite of radioisotope-guided SLND associated with extended pelvic LND (ePLND) is a better technique in detecting affected lymph nodes. Sienna+® tended to accumulate in lymph nodes let them detect at MRI as a T2-weighted strong drop of signal intensity regions. Though, the high sensitivity (96.6%), specificity (95.6%), and the positive predictive value (96.6%); and negative predictive value (95.6%), the low false negative rate (3.4%), and false positive rate (4.4%) determined how the magnometer-guided SLND have higher sensitivity and additional diagnostic value compared to ePLND [47]. In a previous study, Winter et al. considered, besides the high risk group, the intermediate risk of PCa patients and reported the results of preoperative MRI identification of SLN with intraoperative magnetometer-guided SLND. SLND had 100% diagnostic rate, sensitivity equal to 85.7%, 97.2% specificity, 92.3% positive predictive value, 94.9% negative predictive value, and 14.3% false negative rate [10]. SentiMag was employed in the study of Thill et al. to prove the equivalency of this procedure to the gold standard of SLN biopsy in BC with ^{99}mTc-Nanocoll®, a ^{99}mTc-nanocolloid of human albumin, together or without blue dye. SLN were marked with radiopharmaceutical respecting 1- or 2-day protocol and, then, 20 min before SLN biopsy, Sienna+ was injected in the subareolar site. The area was massaged to facilitate the

migration of SPIONs through lymphatic system. The site of injection and axillary area were counted with a gamma probe and SentiMag®. The SLN biopsy continued until the residual activity of the axilla was less than 10%. The LN with less than 10% was not considered SLN while SLN was the LN marked with each method. The detection rate per patient for ^{99}mTc was 97.3%, for Sienna+98%; nodal detection rate (proportion of SLN detected) was 91.8% for radioisotope, 97.3% for Sienna+. The malignancy detection rate per patient was 91.2% for radiopharmaceutical, 91.1% for SPIONs and respectively per node 91.1% and 95.6%. The histological analysis conducted on LN removed gave positive results on 31/146 LN marked with isotope vs. 33/147 LN individuated with SPIONs [48]. Douek et al. proposed further comparison between these two techniques in mammalian cancer. SLN identification was 95.0% with gold standard and 94.4% for SPIONs. The identification rate with gamma probe was 90.6%, with a discordance between the two methods of 6.9%. At histopathology, of 107 LN not detected by isotope, 55 were identified by Sienna+. Twenty-nine LN were identified by ^{99}mTc-Nanocoll® only. SPIONs, however, was limited by false negative because not all the LN identified were detected by gold standard [49, 50]. Staník et al. showed that SPIONs could be used as an alternative to the gold standard to detect the SLN in intermediate and high risk PCa. They performed magnetometer-guided SLND gaining a diagnostic rate of 95% [11].

Not only for PCa, were SPIONs also proposed as tracers in penile cancer too. Using MRI in identifying the SLN after 24 h SPIONs injection, it was obtained hyperintense signal in metastatic SLN on T1 compared to normal tissue since in metastatic SLN there are not reticuloendothelial system (RES) cells in the infiltration cancer areas. At the opposite, non-metastatic SLN, rich in RES cells, contained great quantitative of SPIONs as selectively phagocytized by macrophages, monocytes, and other cells of RES. The study of Tabatabei et al., that used the SPIONs Ferumoxatran-10, reported 100% sensitivity, 97% specificity, 81.2% positive predictive value, and 100% negative predictive value. The small population, however, make larger-scaled study necessary [12, 51] (See Fig. 2).

99mTc-Biphosphonate

Recently, ^{99}mTc-biphosphonate, a radiopharmaceutical used in bones scintigraphy, has been coated with magnetic nanoparticles (MNPs) and proposed as a theragnostic nanoagent [52] (See Fig. 3). The bisphosphonates considered were methylene diphosphonate (MDP) and 1-hydroxyethane-1,1-diphosphonate (HEDP). For better heating ability, only ^{99}mTc-Fe_3O_4-HEDP MNPS studies were performed. After injection in mice tail veins of ^{99}mTc-Fe_3O_4-HEDP MNPs and ^{99}mTc-HEDP, dynamic SPECT studies and planar imaging were acquired by gamma camera with Low energy-High resolution with energy peak setting on 140 keV: MNPs accumulated in liver and spleen and eliminated by the urinary system; ^{99}mTc-HEDP, at the opposite side, showed bone uptake. It suggested that ^{99}mTC-biphosphonate-coated Fe_3O_4 MNPs should be considered as a possible tracer in nuclear medicine, especially if small field of view gamma cameras [65] will be adopted.

Application in MRI and PET

N,N,N-trimethyl chitosan (TMC)-coated MNPs conjugated to S-2-(4-isothiocyanatobenzyl)-1,4,7,10-tetraazacyclododecane tetra acetic acid (DOTA) with bombesin (BN) and radiolabeled with Gallium-68 (^{68}Ga) has been proposed as PET/MRI tracer in detecting BC cells. The radiolabeled SPIONs were selective for the gastrin-releasing peptide (GRP) especially present in human breast tumor cells, line BC T-47D [53, 54]. The reason for the use of BN lies in the fact that BN is a high-affinity amphibian analog of GRP [66]. The DOTA–BN–TMC–MNPs were injected to the normal Balb/C and tumor nude mice model through the tail vein and PET at 30, 60, and 120 min, and pre and post-injection 3 T MRI were performed. In MRI, the images T2-weighted images of tumor lesion appeared darker since the improved contrast. The tracer in aqueous solutions expressed decreased signal intensity at the Fe concentration surge and the T2 relaxivity (r2) estimated was 330.98 mM − 1·s^−1. ^{68}Ga labeling of DOTA–BN–TMC–MNPs was evaluated with PET (See Fig. 4). In this method, it showed high sensitivity and better visibility of tumor at a lower concentration of MNPs (0.62 mg/mL) than MRI [54], also thanks to the high sensitivity of new PET detectors [67, 68]. In a recent study, 6 healthy mechanically ventilated rats underwent MRI before and after the instillation of 4 million SPION-labeled alveolar-like macrophages (ALMs) into their lugs. Hyperpolarized 129 Xe MRI was used to detect SPION-labeled ALMs in the airways after 1 hour. The areas, in which SPION-labeled ALMs localized, appaired as regions of signal loss with a T∗2 decreased to 54.0 ± 7.0% of the baseline after an hour. It could be so used for targeting and tracking of stem cells for the treatment of lung disease [55]. Liu X et al. [56] constructed a brain-tumor-targeting nanoprobe to identify the areas of EGFRvIII-positive glioblastoma in which could be accumulated the SPIONs. They considered the peptide PEPHC1 which binds to epidermal growth factor receptor variant III (EGFRvIII). EGFRvIII is overexpressed in glioblastoma so it was linked to SPIONs to construct the nanoprobe. SPIONs were labeled with Cyanine7.5 NHS ester (Cy7.5), a near infrared fluorescence dye to obtain also an instrument for optical imaging. The NPs were coated then with PEG to minimize the effect of opsonization in bloodstream by immune system. The EGFRvIII positive human glioblastoma cell lines, U87MG, were injected in mice. After 2 weeks, the mice received

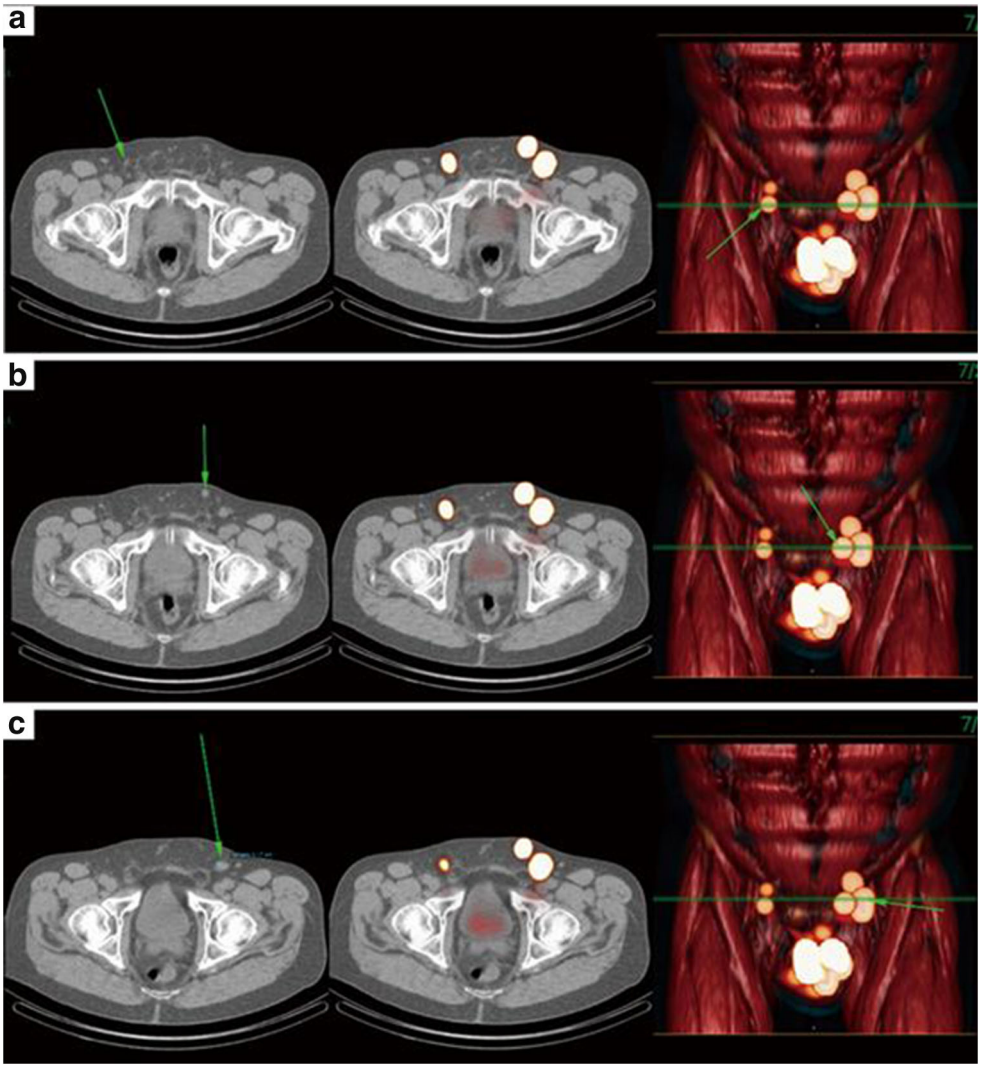

Fig. 2 Uptake of 99mTechnetium-nanocolloid in normal sized right superficial (**A**), left superficial (**B**), and left deep (**C**) inguinal LNs (arrows) seen in SPECT-CT (single-photon emission computed tomography-computed tomography) image

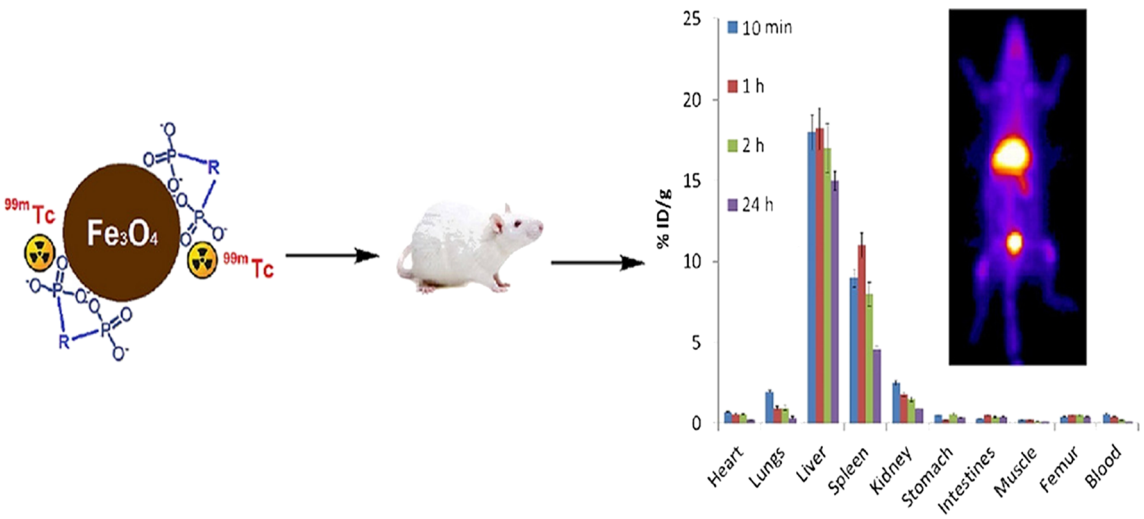

Fig. 3 On the left a representation of ^{99}mTc–Fe_3O_4–HEDP MNPs, on the right a planar image that shows the uptake of the radiopharmaceutical in liver and bladder in a healthy mouse [52]

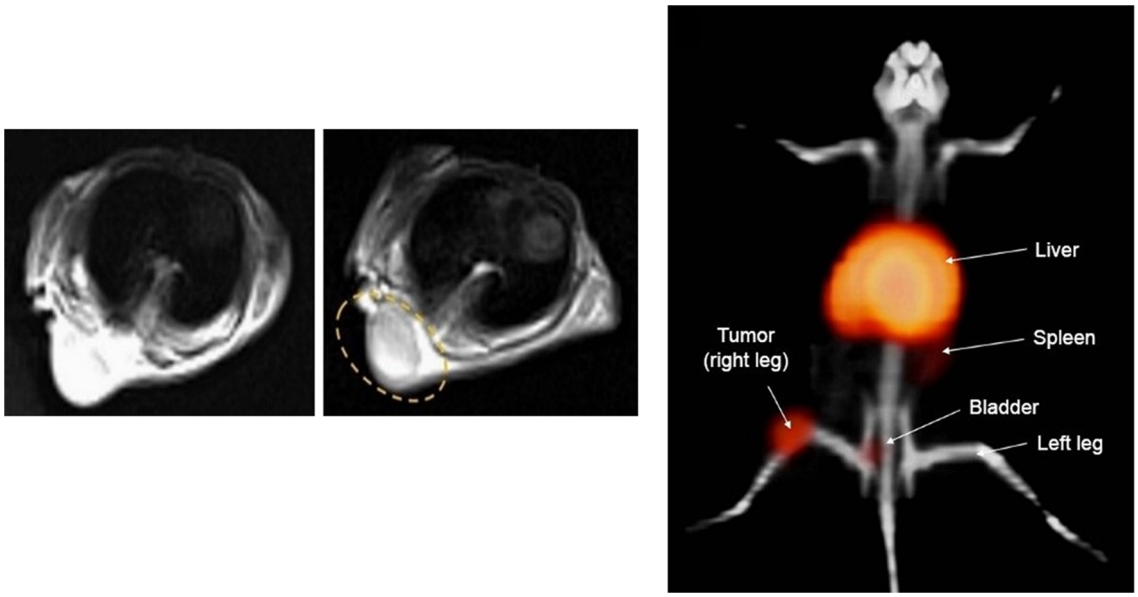

Fig. 4 On the left, an image before injection and in the middle after DOTA–BN–TMC–MNPs injection through the tail vein under the 3 T magnetic field. The uptake of NPs is circled in yellow. In the image on the right, it is shown a PET/CT image of a nude mice with a T-47D BC tumor in the right leg: in yellow the uptake by the liver and tumor after the injection of 3.7 MBq ^{68}Ga–DOTA–BN–TMC–MNPs after 120 min [54]

SPIONs injections, and *T* 2-weighted MR imaging was performed. The brain tumor region appaired as a strong signal area. Fluorescence imaging showed areas of major fluorescence intensity in the brain of the mice injected the SPIONs compared to control mice. It was synthesized also Fe_3O_4-loaded poly(D,L-lactide-co-glycolide) (PLGA) -PEG-aldehyde nanoparticles and proposed them to detect EGFR expressing tumor cells [57].

Toxicity and Adverse Effects

The findings of the SPIONs' use available in the literature are multiple, as the damage to cells, the damage determined by the instability of the compound, the toxicity related to the coating and the poorness of in vivo studies with uncertain effects on human physiology.

Cellular Damage and Compound Instability

Various studies have provided contradicting results. For example, Markides et al. [7] have demonstrated in their study that there were no adverse effects on cellular viability of MSCs at 24 h and 5 days. The proliferation ability of MSCs was maintained over 7 days at Alamar blue metabolic assay. There were no side effects in sheep and there was no evidence of serum c-reactive protein (CRP) increase. On the other side, it was demonstrated that MCF-7 BC cells preserved the viability if they were exposed to NPs. On the contrary, the viability decreased under the 80% if the cells were incubated for 24 h with SPIONs coated with poly(methacrylic acid) (PMAA) or citrate-coated SPIONs (SPIONs-CA). After adding fetal bovine serum (FBS) the viability increased by over 80%. Furthermore, it was proved that uncoated SPIONs get aggregation in water and gave as result a compound with a diameter of approximately 300 nm. After 24 h of incubation in water, uncoated SPIONs and SPIONs-PMAA slightly increased the diameter, while SPIONs-CA aggregated giving a compound with size larger than 3 μm. In phosphate buffered saline (PBS), uncoated SPIONs and SPIONs-CA aggregated forming compounds bigger than 1 μm, while SPIONs-PMAA increased their diameter after 24 h of incubation. In the cell culture environment, all these showed high instability. They aggregated and formed components > 1 μm but, adding FBS to the solution, they reduced their diameter. This phenomenon in the presence of FBS is guaranteed since the serum proteins bound the surface of SPIONs and formed a protein coronas that can inhibit particle aggregation, as confirmed by spectroscopy [14]. It was studied, in addition, the combination of therapeutic ultrasonic waves of 1 MHz intensity and different concentrations of Fe_3O_4 nanoparticles on MCF-7 cell line. It was seen that the cell viability values decreased 20% after 24 h and 25% after 72 h at the concentration of 200 μg/mL of SPIONs [69]. Another effect is that SPIONs induced autophagy and hindered the neovascularization in endothelial progenitor cells [15]. Previously Mahmoudi et al. [70, 71] observed the presence of gas vesicles and an increase of the granularity in SPIONs treated cells. These results confirmed autophagy-mediated cytotoxicity elicited by the NPs. SPIONs has also caused skin staining in 39.9% of patient with BC treated with SPIONs for sentinel node biopsy detection [13]. It seems that SPIONs could have

potential cellular toxicity visible at DNA level directly or by generating reactive oxygen species (ROS). They influence iron homeostasis by up-regulating protein-kinase C (PKC), protein tyrosine-kinase (PTK), and integrins. The expression of pancreatic genes could be changed by SPIONs: they up-regulate the gene expression of beta-2 cells and insulin; SPIONs affect regulatory proteins of cellular cycle up-regulating retinoblastoma protein pRb, B cyclin, D1, and E, cyclin-dependent kinases CDK2 and CDK4, and they down-regulate p21cip1 and p27kip1 [16]. In addition, at high doses SPIONs damage cytoskeleton, in particular tubulin, and dynamic cortical meshwork of F-actin. It leads to decreased cell proliferation [17]. Yet, Jeng et al. demonstrated that Fe_3O_4, Al_2O_3, and TiO_2 had no measurable toxic effects on the cells when the concentrations were less than 200 μg/mL but they had given LDH leakage only at higher doses (> 200 μg/mL) [72]. It was also proved that Fe_3O_4, Al, MoO_3, and TiO_2 had no measurable toxicity at doses between 10 and 50 g/mL. When the concentration reaches levels of 100–250 g/mL, it had been seen changes in size and morphology of BRL 3A rat liver cells [73]. The toxicity of NPs was evident at 100 μg/mL, but not in the range of 0,1–10 μg/mL, also in human glia, human BC, and normal cell lines [74]. Thus, SPIONs seems to be involved in generating ROS that damage proteins, lipid, and DNA, having so a role in carcinogenesis [16]. In particular, Naqvi et al. demonstrated that SPIONs induces ROS-mediated oxidative-stress and apoptosis. They are time and concentration dependent. In fact, the incubation with 500 μg/mL SPIONs reduced the viability of the murine macrophage cell line J774 of 15% in three hours at 3-(4,5-dimethylthiazol-2-yl)- 2,5-diphenyltetrazolium bromide (MTT) assay [75]. HL-7702 cell line (wild type human hepatocyte), similarly, if exposed to uncoated SPIONs, showed nuclear condensation and chromosomal DNA fragmentation, which are markers of apoptosis.

Ways of Damage

The DNA damage was concentration correlated. It increased by 4, 20, 33, and 43% respectively when the concentrations of the SPIONs were 75, 150, 300, and 600 μg/mL. It determined G0/G1 phase arrest. Analogously, the cell membrane was damaged. It was evident by the increase of LDH levels in cells after being incubated with superparamagnetic Fe_3O_4 for 24 h [76]. The principle of oxidative stress caused by SPIONs is related to the producing OH· radical from hydrogen peroxide (H_2O_2) according to Fenton's reaction ($Fe_2+ + H_2O_2 \rightarrow Fe_3+ + OH^- + OH\cdot$). ROS can damage DNA, cell membrane, and organelles' membrane. The damage to the membranes facilitates the release of Ca_2+ and cytochrome C from mitochondria, two inductors of apoptosis. The organelles damaged release iron, that comes in particular from lysosomes and mitochondria, and it accumulates in cytosol. This free iron, helped by ROS, changes the conformation of the proteins determining their aggregation and adding ulterior oxidative stress. It disturbs synaptic function and destroys the dendritic spines of the nervous system and so gives the base for the development of various neuropsychiatric disorders [77]. It was seen that SPIONs could be involved in the genesis of amyloid aggregates. Iron can bind Aβ and deposit as amyloid aggregates that can reduce Fe_3+ to Fe_2+, which by Fenton's reaction, produces further ROS. As result, ROS produce additional aggregation of Aβ. Removal of iron ions from senile plaques reduces plaque toxicity and makes amyloid more soluble. SPIONs could be toxic for SHSY5Y human neuroblastoma cells too. After 24-h exposure to 10 μg/mL of 10 and 30 nm ferric oxide nanoparticles (Fe-NPs), their cellular dopamine content reduced of 68 and 52%, respectively [78]. Pongrac et al. [79] measured levels of reactive oxygen species, intracellular glutathione, mitochondrial membrane potential, cell-membrane potential, DNA damage, and activities of SOD and GPx in murine neural stem cells (NSCs) to understand the possible damage SPIONs-related. They found that glutathione levels in the cells were depleted and demonstrated impaired activities of SOD and GPx. The mitochondria underwent membrane hyperpolarization, the cell-membrane potential was dissipated, and it has seen increased DNA damage, independently by the SPIONs coating. All these effects impaired mitochondrial homeostasis that seemed the principal target of SPIONs. In the human hepatocyte carcinoma cell line (Hep G-2), SPION caused a reduced dose-dependent viability [80], while in human blood cells it increased oxidative stress with dose-dependent DNA damage [81]. The cellular genotoxicity of SPIONs is another crucial theme, studied also in bronchial cell line 16HBE14o-. Evans et al. noticed that SPIONs inducted immunity response against the cellular bronchial line independently if the core was constituted by Fe_2O_3 or Fe_3O_4. They also expressed the opinion that the in vivo studies on a single cellular line precluded the possibility to understand the real damage of MNPs on human beings [82]. The latter study conducted by Gualdani et al. showed an interesting conclusion about the toxic potential of SPIONs. They studied the human ether à go-go-related gene (hERG) channel, a protein that is crucial for the repolarization phase of cardiac action potential [83]. The possible SPIONs influence on hERG channel activity was analyzed. It was investigated if the dimensions, the oxidation state and the coating of SPIONs could affect the interaction with hERG channel. With the help of the patch-clamp recordings, they proved SPIONs inhibition on hERG current. This phenomenon seems to depend on the coating of NPs and a milder effect was evident in SPIONs with covalent coating aminopropylphosphonic acid (APPA). In particular, Fe_2+ ions released from magnetite of the SPIONs can be considered a potential cardiac risk factor because of their capacity to modify hERG gating, leading to a compromise cardiac action potential.

Physicochemical Characteristics of SPIONs and Adverse Effects

There is another aspect to consider. As reported by Singh et al. [16], it is important to obtain good contrast. The SPIONs intravenously injected represent 1.25–5% of the total body iron stores. These particles have a tissue targeted design. It means having high concentration of SPIONs in certain areas could lead to an imbalance of iron homeostasis and then to cytotoxicity and damage to DNA. This could initiate phenomena as cancerogenesis, oxidative stress, epigenetic events, and inflammatory processes [84–87]. It was shown, moreover, that the ^{59}Fe, used to label iron oxide core of SPIONs and to test the integrity of SPIONs in the bloodstream, localized in great levels in the liver and spleen [88]. A further study demonstrated the intracellular accumulation of the ferromagnetic compound in the cultivation of cells with stabilized Fe_3O_4. The uptake by cells of ferromagnetic particles has been observed after 24 and 48 h of incubation. Their intracellular high concentration altered mitochondrial structure leading to the decrease of oxygen uptake rate in the cells [82]. The size and the shape of NPs is another fundamental feature: smaller NPs could accumulate in the cell in higher concentration than the larger ones. Spherical nanoparticles, indeed, degrade more slowly because it has less contact surface available for degradation compared with cubes ones. This problem was stemmed from coating SPIONs with dextran. Dextran binding on the iron of SPIONs is not strong so it tends toward detachment and precipitating with no sufficient evidence of consequence on human health [89, 90]. Uncoated SPIONs, as cited previously, increased the formation of αS aggregation. On the contrary, SPIONs coated with lysine prevent protein aggregation. The potential power of aggregation seen in uncoated SPIONs could be due to their capacity to alter the ionic potential of solutions [77].Wang et al. studied polyethylene glycol and maleic anhydride-coated superparamagnetic iron oxide nanoparticles (Mal-SPIONs) with bovine serum albumin (BSA/Mal-SPIONs) and with Arg-Gly-Asp peptide (RGD/Mal-SPIONs). They valued the distribution of nanoparticles in the brain after the injection of the NPs into the rat substantia nigra. They found a huge quantity of RGD/Mal-SPIONs accumulated in the myelin sheath, dendrites, axon terminals, and mitochondria, and on cell membranes in the brain tissue. BSA/Mal-SPIONs instead accumulated in the myelin sheath, endoplasmic reticulum, axon terminals, Golgi, mitochondria, glial cells, and lysosomes of neurons. In rats which were Mal-SPIONs injected, only the least SPIONs were detected. After the injection, RGD/Mal-SPIONs diffused in different areas as thalamus, frontal cortex, temporal lobe, olfactory bulb, and brain stem, while in the same regions were observed only a few BSA/Mal-SPIONs [91].

Coating Toxicity

There are few studies on human beings, and it is difficult to establish all the effects of SPIONs on human physiology. In one of them, Ferumoxtran-10, an ultra-small superparamagnetic iron oxide particle covered with dextran, has adverse effects. The most frequent in the population of 152 subjects are: headache (5,9%), back pain (5,9%), abdominal pain (3,3%), vasodilation (5,9%), nausea (2,6%), diarrhea (2,0%), injection site reaction (1,3%), chest pain (1,3%), dizziness (1,3%), paresthesia (1,3%), urticaria (5,9%), pruritus (2,6%), and rash (1,3%). The SPIONs infusion was discontinued in four patients because of adverse events [92]. In the phase III trial of ferumoxides, it was discovered back pain as the most frequent adverse reaction (4%) [93]. The reason, strongly studied, perhaps consists in the occlusion of the microvascular structures of the paraspinal muscles, in the spasm of the renal artery or in the allergic reaction. Complement (C) activation is seen in carboxymethyldextran-coated (ferucarbotran, Resosvist®) and dextran-coated (ferumoxtran-10, Sinerem®) SPIONs. Sinerem was a better C activator. It activated the alternative pathway of C at low doses. In particular, the injection of Sinerem in the pig caused a dose-dependent complement activation-related pseudoallergy (CARPA). Both C activating and CARPA were promoted by the tendency to aggregate and the multimodal inhomogeneity distribution of Sinerem, more evident than in Resosvist [94]. Lymphotropic ultra-small SPIONs were used in the detection of SLN metastasis in patients with bladder and prostate cancer. Seven out of 84 patients had mild adverse events as dyspnea and arterial hypertension that required the interruption of the injection [95]. Other adverse events were urticaria, hot flash, headache, swelling of neck and nose, and diarrhea [96]. Veno et al. observed that uncoated-SPIONs reduced the viability of ATII-like A549 human lung cancer cells at exposure concentrations above 20 μg/mL. It was seen already after 3 h of treatment and also after 24 and 48 h of treatment. Conversely, if they were exposed to SiO_2-SPIONs (100 μg/mL), even the highest exposure, there was no evidence of viability reduction. They found in the cells treated, though, ultra-structural and metabolic changes. The damage was evident even at non-cytotoxic concentrations. These alterations can affect the main function of ATII cells, which produce the lung surfactant. SiO_2-SPIONs interfered with lipid metabolism but do not cause cytotoxicity. Moreover, in A549 cells exposed to SiO_2-SPIONs, they found an altered expression of SFTPC gene that encodes the surfactant protein C. SP-C is a hydrophobic protein, expressed only by ATII cells, which role is determinant for the preparation and preservation of the surfactant-film in the alveoli. A deficiency of this protein is responsible of chronic lung disease in humans [97]. In particular, SiO2-SPIONs avoid lamellar body (LBs) biogenesis in A549 cells

and the normal packaging of the surfactant into LBs and stimulated the autophagy in a dose-dependent manner. SiO_2-SPIONs so affect the cells ability to reduce hypophase surface tension, leading to possible lung function impairment [98]. Similarly, Moret et al. noticed that A549 cells expressed a lower amount of SP-C after treatment with PEG-ORMOSIL NPs, condition that can develop airway disorders [99]. Another study valued the effect of PEG surface functionalization with carboxyl and amine terminal modifications of SPIONs after intrapulmonary administration in mice. In acute and sub-acute exposure, both produced an increase of lipid peroxidation in broncho-alveolar lavage fluid (BALF) and lung samples. This phenomenon reverted in a time-dependent manner. DNA damage was seen after the exposition to the NPs and was more evident using negatively charged nanoparticles compared to positively charged nanoparticles. SPIONs determined the gene expression of selected mediators such as CCL-17 and IL-10. SPIONs without surface modification with PEG induced a notable increase of the markers. SPIONs functionalized with PEG-COOH caused a slightly greater increase in gene expression compared to PEG-NH_2-SPIONs. After 1 month all the SPIONs brought about an increase of gene expression of the tested mediators as NOS-2, CXCL-10, CCL-17, CCL-22, and IL-10 [100]. The toxicity of SPION-COOH, but also of plain SPIONs and SPION-NH_2, were analyzed making in relation the expression of genes of hypertrophic cardiomyopathy human heart, BE-2-C brain, and 293 T kidney cell lines through DNA microarrays. As result, SPION-COOH alters the expression of genes which regulate the cell proliferative responses [101, 102]. It was investigated the different effects of uncoated oxide magnetic nanoparticles and the particles (MNPs) labeled with tetraethyl orthosilicate (TEOS), 3-aminopropyltrimethoxysilane (APTMS), or TEOS/APTMS. MNPs caused 5% or less of cytotoxicity in fibrosarcoma cells when their concentration was 500 μg/mL. APTMS-coated MNPs determined more than 10% toxicity against normal cells. Particularly, the genotoxicity of MNPs was dependent on their dose, size, and surface charge, while APTMS- or TEOS/APTMS-coated MNPs induced DNA aberrations in all the cell types studied. All the coatings seem to give oxidative damage [103]. Another study investigated the effects on neuronal cells induced by SPIONs linked with aminosilane or dextran. Aminosilane coated particles altered metabolic activity only at higher concentrations (10%) but did not damage the membrane. Dextran-coated nanoparticles partially reduced viability at higher concentrations (10%) [104]. In a preclinical study of Hoh et al., however, the molecule dextran was studied in the conformation of a synthetic receptor-binding macromolecule, [^{99}mTc]DTPA-mannosyl-dextran. It was tested and there was no evidence of toxicity in rabbit and rats group, in particular, no evidence of hepatic hypertrophy in rats, with unacceptable biodistribution [105]. Aliakbari et al. studied the different effects of polyvinylpyrrolidone (PVP)-coated superparamagnetic iron oxide nanoparticles on BT-474 human BC cell viability. They demonstrated that PVP-SPIONs at 10–100 μg/mL determined the increase of BT474 cell proliferation and, at high concentration, toxic effects. After 72 h of incubation in the concentration of 100 μg/mL, the proliferation of cancer cells raised. Moreover, the toxicity seemed to be in the function of the cellular type and it would be crucial for future toxicological studies [106]. Nevertheless, Maurizi et al. studied the negatively-charged and pegylated nanoparticles and compared to the nanoparticles labeled with negatively-charged carboxydextran. Even though the differences between the surfaces of these particles, they discovered that all these particles have the same biological behavior. It indicated that the magnetic properties were principally influenced by the charge, rather than the coating [107].

SPIONs: A Better Alternative to Lymphoscintigraphy?

A question rises spontaneously if SPIONs can be considered a valid alternative to traditional lymphoscintigraphy or not. Despite all the interesting applications, SPIONs are yet burdened by various critical issues, and we have the necessity of further investigations to have the certainty of their safety on human beings. Nowadays we know that pregnancy is not a contraindication for lymphoscintigraphy, at the opposite of other applications as blue dye. Even the dose given to fetus is irrelevant, especially if the activities are below 10 MBq. The dose of this radiopharmaceutical does not increase the risk of prenatal death, congenital malformation, or mental impairment [108, 109]. Pandit-Taskar et al. measured the absorbed doses in 9-month-pregnant model under the 2-d protocol with this results: 14.9, 0.214, 0.062, 0.151, 0.004, 0.163, 0.075, and 0.014 mGy were calculated in the injected breast, heart, liver, lung, ovaries, thymus, total body, and fetus, respectively, with values for fetus that are below the acceptable limits [110]. Moreover, if we consider the benefit of lymphoscintigraphy of SLN, it is high in pregnant patients with early lesions and clinically or ultrasound negative axilla [111]. The lymphoscintigraphy is a procedure not dangerous for personnel. Yet Stratmann et al. noticed how surgeons should perform 2190 h, scrub nurses 33,333 h and pathologists 14,705 working hours involved in LSN biopsy before surpassing Occupational Safety and Health Administration limits [112]. Brenner et al. measured the radiation exposure, with a mean exposure time of 30 min and 10 min for the surgical team members and the pathology staff, respectively, in 250 operations per year. The finger dose for the surgeon is 10.5 mGy, for the pathologist is 5.55 mGy. The whole-body doses are 0.45 mSv for the surgeon, 0.11 mSv for the operating room nurse, 0.05 mSv for the anesthetist, and 0.21 mSv for the

pathologist. These data confirm that the radiation risk of staff members is very low [113]. The radiation exposure to the staff is not only below the permissible limits, even when high numbers of SN biopsy procedures were performed. Also pregnant staff members that participated in < 100 SN operations stayed below the limits for pregnant [114]. At the state of the art about the toxicology of SPIONs, they should be more investigated to improve the knowledge about the effects on the humans in comparison with lymphoscintigraphy. Lymphoscintigraphy remains a more secure and safer procedure also in particular condition such pregnancy and chronic exposition of operating room staff.

Compliance with Ethical Standards

Conflict of Interest Viviana Frantellizzi, Miriam Conte, Mariano Pontico, Arianna Pani, Roberto Pani, and Giuseppe De Vincentis declare that they have no conflict of interest.

Ethical Approval This work does not contain any studies with human participants or animals performed by any of the authors.

References

1. Lassenberger A, Scheberl A, Stadlbauer A, Stiglbauer A, Helbich T, Reimhult E. Individually stabilized, Superparamagnetic nanoparticles with controlled shell and size leading to exceptional stealth properties and high relaxivities. ACS Appl Mater Interfaces. 2017;9:3343–53.
2. Uthaman S, Lee SJ, Cherukula K, Cho CS, Park IK. Polysaccharide-coated magnetic nanoparticles for imaging and gene therapy. Biomed Res Int. 2015;2015:959175.
3. Liu F, Le W, Mei T, Wang T, Chen L, Lei Y, et al. In vitro and in vivo targeting imaging of pancreatic cancer using a Fe3O4@SiO2 nanoprobe modified with anti-mesothelin antibody. Int J Nanomedicine. 2016;11:2195–207.
4. Tomanek B, Iqbal U, Blasiak B, Abulrob A, Albaghdadi H, Matyas JR, et al. Evaluation of brain tumor vessels specific contrast agents for glioblastoma imaging. Neuro-Oncology. 2012;14:53–63.
5. Yang RM, Fu CP, Fang JZ, Xu XD, Wei XH, Tang WJ, et al. Hyaluronan-modified superparamagnetic iron oxide nanoparticles for bimodal breast cancer imaging and photothermal therapy. Int J Nanomedicine. 2017;12:197–206.
6. Dulinska-Litewka J, Lazarczyk A, Halubiec P, Szafranski O, Karnas K, Karewicz A. Superparamagnetic Iron Oxide Nanoparticles-Current and Prospective Medical Applications. Materials (Basel). 2019;12(4).
7. Markides H, Newell KJ, Rudorf H, Ferreras LB, Dixon JE, Morris RH, et al. Ex vivo MRI cell tracking of autologous mesenchymal stromal cells in an ovine osteochondral defect model. Stem Cell Res Ther. 2019;10:25.
8. Sciarra A, Gentilucci A, Silvestri I, Salciccia S, Cattarino S, Scarpa S, et al. Androgen receptor variant 7 (AR-V7) in sequencing therapeutic agents for castratrion resistant prostate cancer: a critical review. Medicine (Baltimore). 2019;98:e15608.
9. Ricci M, Frantellizzi V, Bulzonetti N, De Vincentis G. Reversibility of castration resistance status after radium-223 dichloride treatment: clinical evidence and review of the literature. Int J Radiat Biol. 2018:1–29.
10. Winter A, Kowald T, Paulo TS, Goos P, Engels S, Gerullis H, et al. Magnetic resonance sentinel lymph node imaging and magnetometer-guided intraoperative detection in prostate cancer using superparamagnetic iron oxide nanoparticles. Int J Nanomedicine. 2018;13:6689–98.
11. Stanik M, Macik D, Capak I, Mareckova N, Lzicarova E, Dolezel J. Sentinel lymph node dissection in prostate cancer using superparamagnetic particles of iron oxide: early clinical experience. Int Urol Nephrol. 2018;50:1427–33.
12. Mehralivand S, van der Poel H, Winter A, Choyke PL, Pinto PA, Turkbey B. Sentinel lymph node imaging in urologic oncology. Transl Androl Urol. 2018;7:887–902.
13. Karakatsanis A, Daskalakis K, Stalberg P, Olofsson H, Andersson Y, Eriksson S, et al. Superparamagnetic iron oxide nanoparticles as the sole method for sentinel node biopsy detection in patients with breast cancer. Br J Surg. 2017;104:1675–85.
14. Mekseriwattana W, Srisuk S, Kriangsaksri R, Niamsiri N, Prapainop K. The impact of serum proteins and surface chemistry on magnetic nanoparticle colloidal stability and cellular uptake in breast cancer cells. AAPS PharmSciTech. 2019;20:55.
15. Zhang L, Jin R, Sun R, Du L, Liu L, Zhang K, et al. Superparamagnetic iron oxide nanoparticles as magnetic resonance imaging contrast agents and induced autophagy response in endothelial progenitor cells. J Biomed Nanotechnol. 2019;15:396–404.
16. Singh N, Jenkins GJ, Asadi R, Doak SH. Potential toxicity of superparamagnetic iron oxide nanoparticles (SPION). Nanotechnol Rev. 2010;1.
17. Patil RM, Thorat ND, Shete PB, Bedge PA, Gavde S, Joshi MG, et al. Comprehensive cytotoxicity studies of superparamagnetic iron oxide nanoparticles. Biochem Biophys Rep. 2018;13:63–72.
18. Ansari MO, Ahmad MF, Shadab GGHA, Siddique HR. Superparamagnetic iron oxide nanoparticles based cancer theranostics: a double edge sword to fight against cancer. J Drug Delivery Sci Technol. 2018;45:177–83.
19. Elias A, Tsourkas A. Imaging circulating cells and lymphoid tissues with iron oxide nanoparticles. Hematology Am Soc Hematol Educ Program. 2009:720–6.
20. Kumar P, Agnihotri S. Synthesis of dox drug conjugation and citric acid stabilized superparamagnetic iron-oxide nanoparticles for drug delivery. Biochem Physiol: Open Access. 2016;01.
21. Wu VM, Huynh E, Tang S, Uskokovic V. Brain and bone cancer targeting by a ferrofluid composed of superparamagnetic iron-oxide/silica/carbon nanoparticles (earthicles). Acta Biomater. 2019;88:422–47.
22. Awada H, Al Samad A, Laurencin D, Gilbert R, Dumail X, El Jundi A, et al. Controlled anchoring of iron oxide nanoparticles on polymeric nanofibers: easy access to core@shell organic-inorganic nanocomposites for magneto-scaffolds. ACS Appl Mater Interfaces. 2019;11:9519–29.
23. Unterweger H, Janko C, Schwarz M, Dezsi L, Urbanics R, Matuszak J, et al. Non-immunogenic dextran-coated superparamagnetic iron oxide nanoparticles: a biocompatible, size-tunable contrast agent for magnetic resonance imaging. Int J Nanomedicine. 2017;12:5223–38.
24. Szpak A, Kania G, Skorka T, Tokarz W, Zapotoczny S, Nowakowska M. Stable aqueous dispersion of superparamagnetic iron oxide nanoparticles protected by charged chitosan derivatives. J Nanopart Res. 2013;15:1372.
25. Thomas RG, Moon MJ, Lee H, Sasikala AR, Kim CS, Park IK, et al. Hyaluronic acid conjugated superparamagnetic iron oxide nanoparticle for cancer diagnosis and hyperthermia therapy. Carbohydr Polym. 2015;131:439–46.
26. Zhao L, Chano T, Morikawa S, Saito Y, Shiino A, Shimizu S, et al. Hyperbranched polyglycerol-grafted superparamagnetic iron oxide nanoparticles: synthesis, characterization, functionalization,

size separation, magnetic properties, and biological applications. Adv Funct Mater. 2012;22:5107–17.
27. Prabhu S, Mutalik S, Rai S, Udupa N, Rao BSS. PEGylation of superparamagnetic iron oxide nanoparticle for drug delivery applications with decreased toxicity: an in vivo study. J Nanopart Res. 2015;17.
28. Thapa B, Diaz-Diestra D, Beltran-Huarac J, Weiner BR, Morell G. Enhanced MRI T 2 relaxivity in contrast-probed anchor-free PEGylated iron oxide nanoparticles. Nanoscale Res Lett. 2017;12:312.
29. Kurtan U, Esir S, Baykal A, Sözeri H. Poly(amidoamine)-grafted superparamagnetic iron oxide nanoparticles: synthesis and characterization. J Supercond Nov Magn. 2014;27:2097–103.
30. Zhang P, Qiao Y, Wang C, Ma L, Su M. Enhanced radiation therapy with internalized polyelectrolyte modified nanoparticles. Nanoscale. 2014;6:10095–9.
31. Huang S-J, Ke J-H, Chen G-J, Wang L-F. One-pot synthesis of PDMAEMA-bound iron oxide nanoparticles for magnetofection. J Mater Chem B. 2013;1:5916.
32. Kurzhals S, Pretzner B, Reimhult E, Zirbs R. Thermoresponsive polypeptoid-coated superparamagnetic iron oxide nanoparticles by surface-initiated polymerization. Macromol Chem Phys. 2017;218:1700116.
33. Sulek S, Mammadov B, Mahcicek DI, Sozeri H, Atalar E, Tekinay AB, et al. Peptide functionalized superparamagnetic iron oxide nanoparticles as MRI contrast agents. J Mater Chem. 2011;21:15157–62.
34. Amiri H, Saeidi K, Borhani P, Manafirad A, Ghavami M, Zerbi V. Alzheimer's disease: pathophysiology and applications of magnetic nanoparticles as MRI theranostic agents. ACS Chem Neurosci. 2013;4:1417–29.
35. Wang Y, Ye F, Jeong EK, Sun Y, Parker DL, Lu ZR. Noninvasive visualization of pharmacokinetics, biodistribution and tumor targeting of poly[N-(2-hydroxypropyl)methacrylamide] in mice using contrast enhanced MRI. Pharm Res. 2007;24:1208–16.
36. Kowalchuk RM, Pollack SR, Corcoran TA. Zeta potential of bone from particle electrophoresis: solution composition and kinetic effects. J Biomed Mater Res. 1995;29:47–57.
37. Al Mahrouqi D, Vinogradov J, Jackson MD. Zeta potential of artificial and natural calcite in aqueous solution. Adv Colloid Interf Sci. 2017;240:60–76.
38. Mahmoudi M, Sant S, Wang B, Laurent S, Sen T. Superparamagnetic iron oxide nanoparticles (SPIONs): development, surface modification and applications in chemotherapy. Adv Drug Deliv Rev. 2011;63:24–46.
39. Sun ZX, Su FW, Forsling W, Samskog PO. Surface characteristics of magnetite in aqueous suspension. J Colloid Interface Sci. 1998;197:151–9.
40. Teja AS, Koh PY. Synthesis, properties, and applications of magnetic iron oxide nanoparticles. Prog Cryst Growth Charact Mater. 2009;55:22–45.
41. Gupta AK, Gupta M. Synthesis and surface engineering of iron oxide nanoparticles for biomedical applications. Biomaterials. 2005;26:3995–4021.
42. Shao C, Liu F, Le W, Mei T, Wang T, Chen L, et al. In vitro and in vivo targeting imaging of pancreatic cancer using a Fe3O4@SiO2 nanoprobe modified with anti-mesothelin antibody. Int J Nanomedicine. 2016;2195.
43. Mahajan S, Koul V, Choudhary V, Shishodia G, Bharti AC. Preparation and in vitro evaluation of folate-receptor-targeted SPION–polymer micelle hybrids for MRI contrast enhancement in cancer imaging. Nanotechnology. 2012;24:015603.
44. Vogel P, Lother S, Ruckert MA, Kullmann WH, Jakob PM, Fidler F, et al. MRI meets MPI: a bimodal MPI-MRI tomograph. IEEE Trans Med Imaging. 2014;33:1954–9.
45. Vaalma S, Rahmer J, Panagiotopoulos N, Duschka RL, Borgert J, Barkhausen J, et al. Magnetic particle imaging (MPI): experimental quantification of vascular stenosis using stationary stenosis phantoms. PLoS One. 2017;12:e0168902.
46. Sekino M, Kuwahata A, Ookubo T, Shiozawa M, Ohashi K, Kaneko M, et al. Handheld magnetic probe with permanent magnet and hall sensor for identifying sentinel lymph nodes in breast cancer patients. Sci Rep. 2018;8.
47. Winter A, Engels S, Reinhardt L, Wasylow C, Gerullis H, Wawroschek F. Magnetic marking and intraoperative detection of primary draining lymph nodes in high-risk prostate cancer using superparamagnetic iron oxide nanoparticles: additional diagnostic value. Molecules. 2017;22:2192.
48. Thill M, Kurylcio A, Welter R, van Haasteren V, Grosse B, Berclaz G, et al. The central-European SentiMag study: sentinel lymph node biopsy with superparamagnetic iron oxide (SPIO) vs. radioisotope. Breast. 2014;23:175–9.
49. Douek M, Klaase J, Monypenny I, Kothari A, Zechmeister K, Brown D, et al. Sentinel node biopsy using a magnetic tracer versus standard technique: the SentiMAG multicentre trial. Ann Surg Oncol. 2013;21:1237–45.
50. Ahmed M, Purushotham AD, Douek M. Novel techniques for sentinel lymph node biopsy in breast cancer: a systematic review. Lancet Oncol. 2014;15:e351–e62.
51. Tabatabaei S, Harisinghani M, McDougal WS. Regional lymph node staging using lymphotropic nanoparticle enhanced magnetic resonance imaging with ferumoxtran-10 in patients with penile cancer. J Urol. 2005;174:923–7.
52. Mirković M, Radović M, Stanković D, Milanović Z, Janković D, Matović M, et al. 99mTc–bisphosphonate–coated magnetic nanoparticles as potential theranostic nanoagent. Mater Sci Eng C. 2019;102:124–33.
53. Lee CM, Jeong HJ, Cheong SJ, Kim EM, Kim DW, Lim ST, et al. Prostate cancer-targeted imaging using magnetofluorescent polymeric nanoparticles functionalized with bombesin. Pharm Res. 2010;27:712–21.
54. Hajiramezanali M, Atyabi F, Mosayebnia M, Akhlaghi M, Geramifar P, Jalilian AR, et al. (68)Ga-radiolabeled bombesin-conjugated to trimethyl chitosan-coated superparamagnetic nanoparticles for molecular imaging: preparation, characterization and biological evaluation. Int J Nanomedicine. 2019;14:2591–605.
55. Riberdy V, Litvack M, Stirrat E, Couch M, Post M, Santyr GE. Hyperpolarized (129) Xe imaging of embryonic stem cell-derived alveolar-like macrophages in rat lungs: proof-of-concept study using superparamagnetic iron oxide nanoparticles. Magn Reson Med 2019.
56. Liu X, Du C, Li H, Jiang T, Luo Z, Pang Z, et al. Engineered superparamagnetic iron oxide nanoparticles (SPIONs) for dual-modality imaging of intracranial glioblastoma via EGFRvIII targeting. Beilstein J Nanotechnol. 2019;10:1860–72.
57. Salehnia Z, Shahbazi-Gahrouei D, Akbarzadeh A, Baradaran B, Farajnia S, Naghibi M. Synthesis and characterisation of iron oxide nanoparticles conjugated with epidermal growth factor receptor (EGFR) monoclonal antibody as MRI contrast agent for cancer detection. IET Nanobiotechnol. 2019;13:400–6.
58. Ordóñez NG. Application of mesothelin immunostaining in tumor diagnosis. Am J Surg Pathol. 2003;27:1418–28.
59. Multhoff G, Botzler C, Wiesnet M, Müller E, Meier T, Wilmanns W, et al. A stress-inducible 72-kDa heat-shock protein (HSP72) is expressed on the surface of human tumor cells, but not on normal cells. Int J Cancer. 1995;61:272–9.
60. Akaogi K, Okabe Y, Sato J, Nagashima Y, Yasumitsu H, Sugahara K, et al. Specific accumulation of tumor-derived adhesion factor in tumor blood vessels and in capillary tube-like structures of cultured vascular endothelial cells. Proc Natl Acad Sci. 1996;93:8384–9.

61. Croix BS. Genes expressed in human tumor endothelium. Science. 2000;289:1197–202.
62. Pen A, Moreno MJ, Martin J, Stanimirovic DB. Molecular markers of extracellular matrix remodeling in glioblastoma vessels: microarray study of laser-captured glioblastoma vessels. Glia. 2007;55:559–72.
63. Cai W, Chen K, Mohamedali KA, Cao Q, Gambhir SS, Rosenblum MG, Chen X, PET of vascular endothelial growth factor receptor expression. J Nucl Med 2006; 47 (12): 2048-56.
64. Kaul MG, Mummert T, Jung C, Salamon J, Khandhar AP, Ferguson RM, et al. In vitro and in vivo comparison of a tailored magnetic particle imaging blood pool tracer with Resovist. Phys Med Biol. 2017;62:3454–69.
65. Polito C, Pani R, Frantellizzi V, De Vincentis G, Pellegrini R. Imaging performances of a small FoV gamma camera based on CRY018 scintillation crystal. Nuclear Instrum Methods Phys Res A: Accelerators, Spectrom, Detect Assoc Equip. 2018;912:33–5.
66. Spindel ER, Bombesin Peptides. Handbook of Biologically Active Peptides. 2013;326–30.
67. Cinti MN, Scafe R, Bennati P, Lo Meo S, Frantellizzi V, Pellegrini R, et al. Innovative LuYAP:Ce array for PET imaging. J Instrum. 2017;12.
68. Polito C, Pani R, Trigila C, Cinti MN, Fabbri A, Frantellizzi V, et al. Imaging characterization of a new gamma ray detector based on CRY019 scintillation crystal for PET and SPECT applications. J Instrum. 2017;12.
69. Ebrahimi Fard A, Zarepour A, Zarrabi A, Shanei A, Salehi H. Synergistic effect of the combination of triethylene-glycol modified Fe 3 O 4 nanoparticles and ultrasound wave on MCF-7 cells. J Magn Magn Mater. 2015;394:44–9.
70. Mahmoudi M, Simchi A, Vali H, Imani M, Shokrgozar MA, Azadmanesh K, et al. Cytotoxicity and cell cycle effects of bare and poly(vinyl alcohol)-coated Iron oxide nanoparticles in mouse fibroblasts. Adv Eng Mater. 2009;11:B243–B50.
71. Mahmoudi M, Simchi A, Imani M, Shokrgozar MA, Milani AS, Hafeli UO, et al. A new approach for the in vitro identification of the cytotoxicity of superparamagnetic iron oxide nanoparticles. Colloids Surf B: Biointerfaces. 2010;75:300–9.
72. Jeng HA, Swanson J. Toxicity of metal oxide nanoparticles in mammalian cells. J Environ Sci Health A Tox Hazard Subst Environ Eng. 2006;41:2699–711.
73. Hussain SM, Hess KL, Gearhart JM, Geiss KT, Schlager JJ. In vitro toxicity of nanoparticles in BRL 3A rat liver cells. Toxicol in Vitro. 2005;19:975–83.
74. Ankamwar B, Lai TC, Huang JH, Liu RS, Hsiao M, Chen CH, et al. Biocompatibility of Fe(3)O(4) nanoparticles evaluated by in vitro cytotoxicity assays using normal, glia and breast cancer cells. Nanotechnology. 2010;21:75102.
75. Naqvi S, Samim M, Abdin M, Ahmed FJ, Maitra A, Prashant C, et al. Concentration-dependent toxicity of iron oxide nanoparticles mediated by increased oxidative stress. Int J Nanomedicine. 2010;5:983–9.
76. Xin-Li L, Shu-Hua Z, Long Z, Gui-Qin H, Sun ZW, Yang W. Dose-dependent Cytotoxicity and Oxidative Stress Induced by "Naked" Fe 3 O 4 Nanoparticles in Human Hepatocyte. 2012; 28.
77. Yarjanli Z, Ghaedi K, Esmaeili A, Rahgozar S, Zarrabi A. Iron oxide nanoparticles may damage to the neural tissue through iron accumulation, oxidative stress, and protein aggregation. BMC Neurosci. 2017;18:51.
78. Imam SZ, Lantz-McPeak SM, Cuevas E, Rosas-Hernandez H, Liachenko S, Zhang Y, et al. Iron oxide nanoparticles induce dopaminergic damage: in vitro pathways and in vivo imaging reveals mechanism of neuronal damage. Mol Neurobiol. 2015;52:913–26.
79. Pongrac IM, Pavicic I, Milic M, Brkic Ahmed L, Babic M, Horak D, et al. Oxidative stress response in neural stem cells exposed to different superparamagnetic iron oxide nanoparticles. Int J Nanomedicine. 2016;11:1701–15.
80. Riasat R, Nie G. Synthesis and characterization of nontoxic hollow Iron oxide (α-Fe2O3) nanoparticles using a simple hydrothermal strategy. J Nanomater. 2016;2016:1–7.
81. Sonmez E, Aydin E, Turkez H, Özbek E, Togar B, Meral K, et al. Cytotoxicity and genotoxicity of iron oxide nanoparticles: an in vitro biosafety study. Arch Biol Sci. 2016;68:41–50.
82. Evans SJ, Clift MJD, Singh N, Wills JW, Hondow N, Wilkinson TS, et al. In vitro detection of in vitro secondary mechanisms of genotoxicity induced by engineered nanomaterials. Part Fibre Toxicol. 2019;16:8.
83. Gualdani R, Guerrini A, Fantechi E, Tadini-Buoninsegni F, Moncelli MR, Sangregorio C. Superparamagnetic iron oxide nanoparticles (SPIONs) modulate hERG ion channel activity. Nanotoxicology 2019; 1-13.
84. Bulte JW, Douglas T, Witwer B, Zhang SC, Strable E, Lewis BK, et al. Magnetodendrimers allow endosomal magnetic labeling and in vivo tracking of stem cells. Nat Biotechnol. 2001;19:1141–7.
85. Veranth JM, Kaser EG, Veranth MM, Koch M, Yost GS. Cytokine responses of human lung cells (BEAS-2B) treated with micron-sized and nanoparticles of metal oxides compared to soil dusts. Part Fibre Toxicol. 2007;4:2.
86. Hafeli UO, Riffle JS, Harris-Shekhawat L, Carmichael-Baranauskas A, Mark F, Dailey JP, et al. Cell uptake and in vitro toxicity of magnetic nanoparticles suitable for drug delivery. Mol Pharm. 2009;6:1417–28.
87. Singh N. Conference scene - nanotoxicology: health and environmental impacts. Nanomedicine (London). 2009;4:385–90.
88. Wang H, Kumar R, Nagesha D, Duclos RI Jr, Sridhar S, Gatley SJ. Integrity of (111)in-radiolabeled superparamagnetic iron oxide nanoparticles in the mouse. Nucl Med Biol. 2015;42:65–70.
89. Jung CW. Surface properties of superparamagnetic iron oxide MR contrast agents: ferumoxides, ferumoxtran, ferumoxsil. Magn Reson Imaging. 1995;13:675–91.
90. McCarthy JR, Weissleder R. Multifunctional magnetic nanoparticles for targeted imaging and therapy. Adv Drug Deliv Rev. 2008;60:1241–51.
91. Wang S, Zhang B, Su L, Nie W, Han D, Han G, et al. Subcellular distributions of iron oxide nanoparticles in rat brains affected by different surface modifications. J Biomed Mater Res A. 2019;107:1988–98.
92. Anzai Y, Piccoli CW, Outwater EK, Stanford W, Bluemke DA, Nurenberg P, et al. Evaluation of neck and body metastases to nodes with ferumoxtran 10-enhanced MR imaging: phase III safety and efficacy study. Radiology. 2003;228:777–88.
93. Ros PR, Freeny PC, Harms SE, Seltzer SE, Davis PL, Chan TW, et al. Hepatic MR imaging with ferumoxides: a multicenter clinical trial of the safety and efficacy in the detection of focal hepatic lesions. Radiology. 1995;196:481–8.
94. Fulop T, Nemes R, Meszaros T, Urbanics R, Kok RJ, Jackman JA, et al. Complement activation in vitro and reactogenicity of low-molecular weight dextran-coated SPIONs in the pig CARPA model: correlation with physicochemical features and clinical information. J Control Release. 2018;270:268–74.
95. Birkhauser FD, Studer UE, Froehlich JM, Triantafyllou M, Bains LJ, Petralia G, et al. Combined ultrasmall superparamagnetic particles of iron oxide-enhanced and diffusion-weighted magnetic resonance imaging facilitates detection of metastases in normal-sized pelvic lymph nodes of patients with bladder and prostate cancer. Eur Urol. 2013;64:953–60.
96. Triantafyllou M, Studer UE, Birkhauser FD, Fleischmann A, Bains LJ, Petralia G, et al. Ultrasmall superparamagnetic particles of iron oxide allow for the detection of metastases in normal sized pelvic lymph nodes of patients with bladder and/or prostate cancer. Eur J Cancer. 2013;49:616–24.

97. Perez-Gil J, Weaver TE. Pulmonary surfactant pathophysiology: current models and open questions. Physiology (Bethesda). 2010;25:132–41.
98. Kononenko V, Erman A, Petan T, Krizaj I, Kralj S, Makovec D, et al. Harmful at non-cytotoxic concentrations: SiO2-SPIONs affect surfactant metabolism and lamellar body biogenesis in A549 human alveolar epithelial cells. Nanotoxicology. 2017;11:419–29.
99. Moret F, Selvestrel F, Lubian E, Mognato M, Celotti L, Mancin F, et al. PEGylation of ORMOSIL nanoparticles differently modulates the in vitro toxicity toward human lung cells. Arch Toxicol. 2015;89:607–20.
100. Al Faraj A, Shaik AP, Shaik AS. Effect of surface coating on the biocompatibility and in vivo MRI detection of iron oxide nanoparticles after intrapulmonary administration. Nanotoxicology. 2015;9:825–34.
101. Mahmoudi M, Laurent S, Shokrgozar MA, Hosseinkhani M. Toxicity evaluations of superparamagnetic iron oxide nanoparticles: cell "vision" versus physicochemical properties of nanoparticles. ACS Nano. 2011;5:7263–76.
102. Laurent S, Saei AA, Behzadi S, Panahifar A, Mahmoudi M. Superparamagnetic iron oxide nanoparticles for delivery of therapeutic agents: opportunities and challenges. Expert Opin Drug Deliv. 2014;11:1449–70.
103. Yang WJ, Lee JH, Hong SC, Lee J, Lee J, Han DW. Difference between toxicities of Iron oxide magnetic nanoparticles with various surface-functional groups against human normal fibroblasts and fibrosarcoma cells. Materials (Basel). 2013;6:4689–706.
104. Rivet CJ, Yuan Y, Borca-Tasciuc DA, Gilbert RJ. Altering iron oxide nanoparticle surface properties induce cortical neuron cytotoxicity. Chem Res Toxicol. 2012;25:153–61.
105. Hoh CK, Wallace AM, Vera DR. Preclinical studies of [(99m)Tc]DTPA-mannosyl-dextran. Nucl Med Biol. 2003;30:457–64.
106. Aliakbari M, Mohammadian E, Esmaeili A, Pahlevanneshan Z. Differential effect of polyvinylpyrrolidone-coated superparamagnetic iron oxide nanoparticles on BT-474 human breast cancer cell viability. Toxicol in Vitro. 2019;54:114–22.
107. Maurizi L, Papa AL, Dumont L, Bouyer F, Walker P, Vandroux D, et al. Influence of surface charge and polymer coating on internalization and biodistribution of polyethylene glycol-modified Iron oxide nanoparticles. J Biomed Nanotechnol. 2015;11:126–36.
108. Buscombe J, Paganelli G, Burak ZE, Waddington W, Maublant J, Prats E, et al. Sentinel node in breast cancer procedural guidelines. Eur J Nucl Med Mol Imaging. 2007;34:2154–9.
109. Khera SY, Kiluk JV, Hasson DM, Meade TL, Meyers MP, Dupont EL, et al. Pregnancy-associated breast cancer patients can safely undergo lymphatic mapping. Breast J. 2008;14:250–4.
110. Pandit-Taskar N, Dauer LT, Montgomery L, St Germain J, Zanzonico PB, Divgi CR. Organ and fetal absorbed dose estimates from 99mTc-sulfur colloid lymphoscintigraphy and sentinel node localization in breast cancer patients. J Nucl Med. 2006;47:1202–8.
111. Gentilini O, Cremonesi M, Toesca A, Colombo N, Peccatori F, Sironi R, et al. Sentinel lymph node biopsy in pregnant patients with breast cancer. Eur J Nucl Med Mol Imaging. 2010;37:78–83.
112. Stratmann SL, McCarty TM, Kuhn JA. Radiation safety with breast sentinel node biopsy. Am J Surg. 1999;178:454–7.
113. Brenner W, Ostertag H, Peppert E, Czech N, Kampen WU, Muhle C, et al. Radiation exposure to the personnel in the operating room and in the pathology due to SLN detection with Tc-99m-nanocolloid in breast cancer patients. Nuklearmedizin. 2000;39:142–5.
114. Klausen TL, Chakera AH, Friis E, Rank F, Hesse B, Holm S. Radiation doses to staff involved in sentinel node operations for breast cancer. Clin Physiol Funct Imaging. 2005;25:196–202.